Efficient Underground Object Detection for Ground Penetrating Radar Signals

İbrahim Meşecan[1,2] and İhsan Ömür Bucak[3]
[1]Computer Engineering Department, Mevlana University, Konya, Turkey
[2]Computer Engineering Department, Epoka University, Tirana Albania
[3]Department of Electrical and Electronics Engineering, Melikşah University, Kayseri, Turkey,

ABSTRACT

Ground Penetrating Radar (GPR) is one of the common sensor system for underground inspection. GPR emits electromagnetic waves which can pass through objects. The reflecting waves are recorded and digitized, and then, the B-scan images are formed. According to the properties of scanning object, GPR creates higher or lower intensity values on the object regions. Thus, these changes in signal represent the properties of scanning object. This paper proposes a 3-step method to detect and discriminate landmines: 1) n-row average-subtraction (NRAS) 2) Min-max normalization 3) image scaling. Proposed method has been tested using 3 common algorithms from the literature. According to the results, it has increased Object Detection Ratio (ODR) and Positive Object Discrimination (POD) significantly. For Artificial Neural Networks (ANN), POD has increased from 77.4% to 87.7%. And, it has increased from 37.8% to 80.2%, for Support Vector Machines (SVM).

Keywords: GPR, B-scan images, Image processing, Object detection, n-row average subtraction.

1. INTRODUCTION

First usage of landmines dates back to 13th century when Chinese used contact fused land mines to stop Mongols[1]. Land mines are mostly placed between countries in war times. It is reported that more than a hundred million land mines exist in more than 80 countries[2]. Because of landmines[3], more people are being killed or injured every year. After the start of World Wars, many countries started using land mines more. Underground object detection has become more important[1] as a result.

The detection of land mines problem is a difficult process due to many factors: large variety of land mine types, different terrain, or weather conditions, and human or natural waste[4], etc. Because of the fact that many modern land mines contain little or no metal, traditional field detectors cannot produce any good results[5]. Some sensors for underground inspection include acoustics and quadruple resonance, GPR, electro-magnetic induction sensing (EMI) and neutron backscattering[6]. Recently, GPR has become one of the commonly used sensors for many[3,7-9] researchers.

Sinha and Mehta[9] review the nature of minefields and evaluate several landmine detection methods. In conclusion, they state that GPR offers better detection possibilities. Mine detection using GPR data and signal processing techniques has a long history[10]. The signals

gathered from sensing devices are processed using different signal and image processing techniques.

Some methods applied for mine detection are background removal[11], Hidden Markov Models (HMMs)[12,13], using frequency domain features[3], Fuzzy K-Nearest Neighbors[4], Edge Histogram Descriptors[14], and adaptive approaches for anomaly detection[15], etc.

Due to the real-time requirements many researchers developed two staged algorithms: pre-screening and feature-processing stages. The first phase aims to detect potential interest points quickly and it passes them to a more detailed algorithmic processor. Torrione et al.[6] state that feature-based processor helps to reduce False Alarm Rate (FAR) significantly while keeping the probability of detection the same.

Gader et al.[8] report that 'feature based methods outperformed energy detectors'. Frigui et al.[3,14] propose to use Edge Histogram Descriptors (EHD). They use a simple edge operator to identify and group edges. They claim that EHD helps to reduce false alarm rate without effecting the detection rate.

In this paper, a 3-step method is proposed to locate and discriminate land mines: 1) processing B-scan images according n-row average subtraction 2) Using Min-max normalization for the intensity values and 3) Scaling images. Then, the paper tests and analyzes proposed method using 3 common algorithms from the literature.

The rest of the paper is organized as follows: Section 2 explains the properties of the dataset used and NRAS. Section 3 presents implementation details and the results. The paper finishes with conclusions.

2. METHODOLOGY

Before discussing about NRAS, the properties of the dataset need to be explained.

2.1 Dataset used

The dataset has been provided by The Information Technologies Institute of the Scientific and Technological Research Council of Turkey (TUBİTAK) - Gebze, Kocaeli. The data has been collected:

- using soft soil and 1 GHz GPR signals,
- for two types of objects: metal and plastic,
  - 10 - 25 cm diameter and 4 cm high metal disc landmines,
  - 5-liter standard cylindrical plastic container land mines,
- for different object depths: 3, 10, 20, 30 and 40 cm,
- and for different antenna heights: 5, 10, 15 and 20 cm.

There are also some images which have been captured when there is no test object.

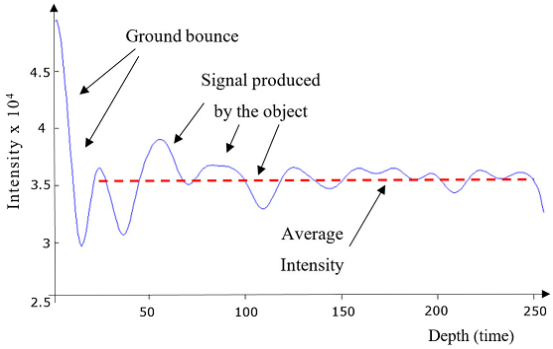

Figure 1: A-scan signal

First, A-scan signals are captured[16,17], Figure 1. As it is seen from the figure, there is high fluctuation in the first few rows in depth direction where the signal passes from air to the ground. This part of the signal is called ground bounce. It is also important to note that the average intensity is very high (dashed line).

To have better Signal to Noise Ratio (SNR), every point is scanned several times (R - usually 4 or 8). Later, the signal is digitized and averaged (Eq. 1)[16]. For better detection, the signals have been digitized using 2-byte intensity resolution (from 0 to 65535).

$$a_A(x,y,z) = \frac{1}{R}\sum_{r=1}^{R} a(x,y,z) \qquad (1)$$

where R is the number of A-scan signals taken and $a_A(x,y,z)$ is the averaged A-scan signal over R scans.

Finally, A-scan signals are combined together to form B-scan images. Figure 2 shows two B-scan images where image (b) contains dashed rectangle to highlight the object region from the image (a).

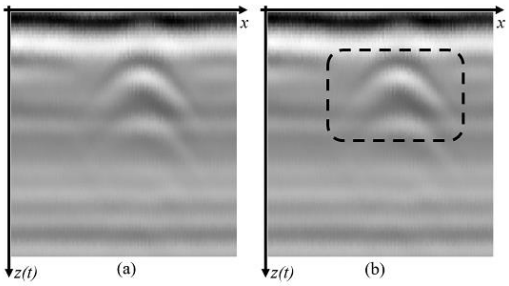

Figure 2: B-scan image captured for a metal object which is buried under 3 cm.

Thus, 10 B-scan images have been collected for every object depth and antenna height (height of antenna from the ground). Then, the images have been classified into three categories;

1. True positive (TP) images: images which contain query object whose type and position are known,
2. True negative (TN) images: images which do not contain any query object,
3. Images which contain a query object but whose position are not recorded.

The sensing limit of GPR devices change according to the frequency used[18]. In many other researches[7,12,19], the objects are buried less than 10 inches deep. But in this research, there are some objects which are buried 30 and 40 cm deep. When an object goes beyond the sensing limits of GPR sensors, the object cannot be captured in the image. This can be seen in Figure 3 through the images in which the object depths are 20 - 30 cm and antenna heights are 10, 15 and 20 cm.

For every object depth, images have been acquired using different antenna heights. Both, height of antenna from the ground and the buried object depth effect the detection. It can be seen from Figure 3 that for the same object depth (rows), when the height of antenna changes (columns), the object is detected in deeper positions in the image. In the figure, although the object used in all scans is the same object, it is captured in deeper positions in the images. After a point the object disappears from the visible scene of the image. Thus, the images which are out of the detection limits of GPR have been used as TN images.

As a result, for exact comparison of the results, the images whose exact object positions are not recorded have not been used in the tests. And, we have the following number of images in tests:

1. 310 TP images:
   a. 250 metal mines,
   b. 60 plastic mines.
2. 180 TN images.

2.2 n-row average subtraction (NRAS)

Row Mean Subtraction (RMS) is a common method in image processing[20,21]. Hence, row mean is too much effected from the fluctuations in the current row, RMS provides lower results compared to NRAS for many algorithms tested.

When GPR signals pass through a medium with the same properties, they are reflected back with the same

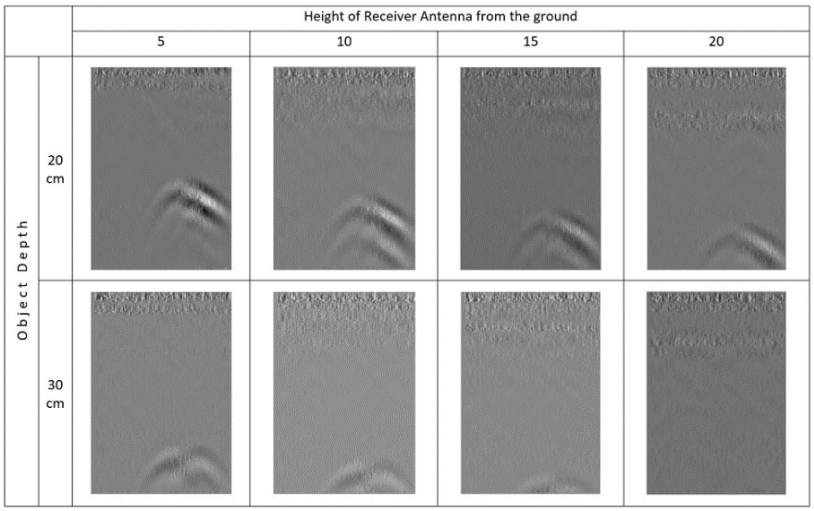

Figure 3: GPR signals taken from different depths and antenna heights.

signal levels. This produces same signal levels like beam bands for the entire row which can be seen in Figure 4 on the rows from 140 to 200. When beams pass through a different medium, they are returned with different peaks (higher intensity levels on a region compared to the pixels around) or holes in the signal. These peaks and holes serve as a signature of the object being captured.

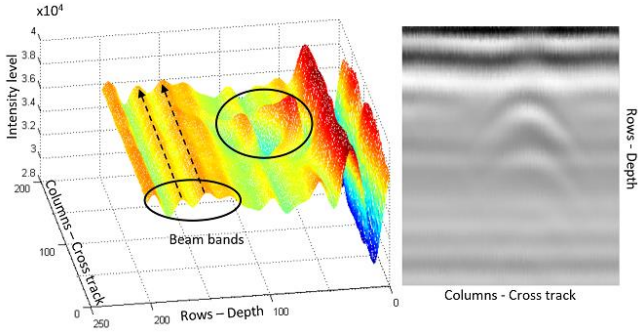

Figure 4: Coloring images according to the intensity levels.

The parallel bands show the extra information that does not contain object specific information. The peaks and holes appear on the object regions.

Using these parallel bands, the images can be normalized. As an example, for processing according to 3-row average, the average of the current, preceding and the next rows is subtracted from every pixel intensities of the current row. Then, the real object information (peaks and holes) is left and extra information is removed from the signal:

$$cra = \mu(\mu_{r-1}, \mu_r, \mu_{r+1})$$
$$a(x, z_r) = a(x, z_r) - cra \quad (2)$$

where μ_r is the average of r^{th} row and *cra* is the average of current, preceding and the next row averages. Later, *cra* is subtracted from every element of the current row.

Figure 5 shows three images: a) a metal object buried under 10 cm (for a better visualization, the first fifty rows have been removed), b) after processing according to 3-row average c) after resizing image to 50%. As it can be seen from the figure, 3-row average subtraction method preserves most of signal properties while removing extra information. Furthermore, the signatures are preserved even after significant image scaling[22].

2.3 Runtime complexity

NRAS calculates the average of every row. Then, n-row average is subtracted from row every element. Therefore, it uses $2hw$ operations where *h* and *w* are the dimensions of 2D B-scan image. After NRAS, data is Min-max normalized $2hw$ operations.

As a result, the runtime complexity of the proposed uses $4hw$ operations. Thus, the runtime complexity is $O(hw)$. This complexity is the same for the background removal method[11] proposed by Sezgin et al. However, they use $56hw$ operations for a similar operation.

As a result, the method shows reasonably better runtime performance. By the use of image scaling, the method is promising for online detection.

3. IMPLEMENTATION AND RESULTS

The effects of NRAS have been analyzed using three common algorithms: ANN, SVM, and KMeans.

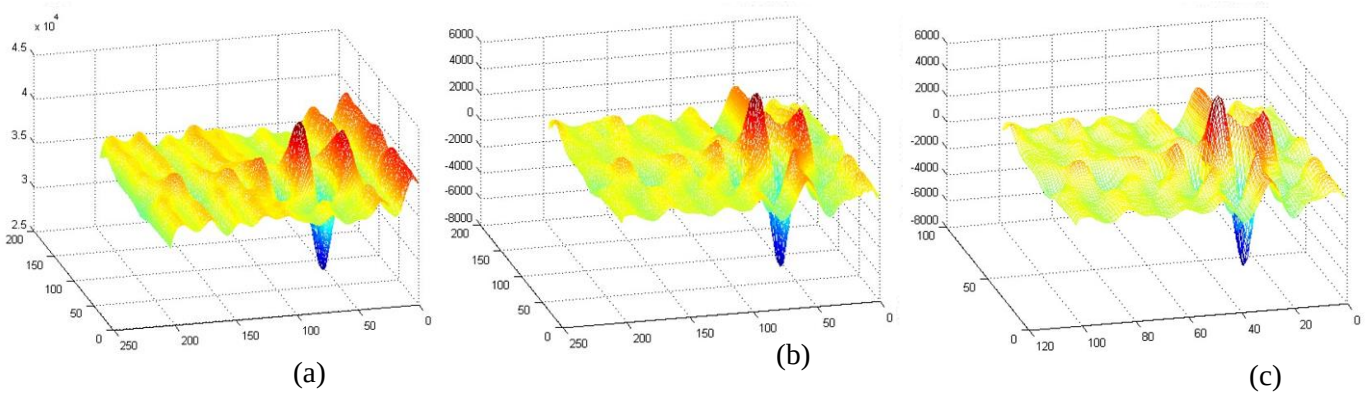

(a) (b) (c)

Figure 5: Images before and after processing.

For comparison of the results, algorithms have been tested using 4 test settings:

1. No Normalization (NN): raw images without any operation.
2. Min-max normalization (MM): The image intensity is normalized to the range from 0 to 1. And, the image crops are taken for testing.
3. NRAS: (where n is an odd number between 1 and 7). Entire image is processed according to NRAS. Then, the image crops are taken.
4. 3-row average + Min-max normalization (3RM): Entire image is first processed according to 3-row average subtraction. Then, the image is Min-max normalized to the range from 0 to 1. And, the image crops are taken.

In the end, all tests have been implemented using 3 different image scales[22] 33%, 25%, and 20%.

There are 180 negative (TN) B-scan images, 250 B-scan images which contain a metal landmine object, and 60 B-scan images which contain a plastic landmine object. Every B-scan image is 256-by-180 pixel image where the 256 rows represent the depth. Objects usually create a 60-by-90 signature in the image.

Because dataset is small, 60-by-90 image crops have been taken from the existing negative images. Hence entire image is negative (no query object in it), any part of the image can be cropped as a new negative image. Thus, 6 image crops have been taken from random coordinates of each TN image. As a result, a set of $(180 \times 6) = 1080$ TN images have been produced.

However, TP images cannot be reproduced with the way negative images have been reproduced. To produce more test sets, the program was run 10 times. In every run, the order of images have been shuffled randomly to construct different test and data sets: as a total of $\big(10 \times (1080 + 250 + 60)\big) = 13900$ test images.

3.1 Performance measurement and formulas

For many researchers, KMeans is among top ten algorithms in Data mining[23]. It is an unsupervised clustering algorithm. However, because the number of test objects in three classes are very different, KMeans has been used like a classifier in the tests below. As there are only 60 plastic test objects, the cluster with the most number of items (e.g. a cluster with 1000 items) cannot be the cluster for plastic objects, the cluster has been assigned as negative. Later, the objects assigned to the cluster have been verified if they are assigned correctly or not. By this way, the clusters of KMeans have been used like a classifier.

Table 1 has been produced with the following conditions:

- KMeans with K=3; three classes: metal objects, plastic objects and None exists,
- for 1080 TN and 310 TP (250 metal and 60 plastic objects),
- 60-by-90 image crops have been scaled to 25%,
- program was run 10 times,
- using MM (test setting 2).

Table 1: Object discrimination for KMeans.

		Object detected		
		Metal	Plastic	Nothing
Actual Object	Metal	1156	789	555
	Plastic	91	85	424
	Nothing	1850	2281	6669

KMeans has identified 1156 metal objects correctly as metal; 789 metal objects have been misclassified as plastic and 555 metal objects have been misclassified as Nothing. Thus, $(1156 + 85 + 6669) = 7910$ images out of 13900 have been identified correctly. That is 56.9% of all objects have been classified correctly.

Table 2: Truth table for the confusion matrix.

		Object detected		
		Metal	Plastic	Nothing
Actual Object	Metal	TP	FC	FN
	Plastic	FC	TP	FN
	Nothing	FP	FP	TN

Table 2 shows the truth table for the confusion matrix. When an object is identified correctly as in the dataset, it is count as TP or TN. If a positive image classified as negative, then it is false negative (FN).

When a metal object is classified as plastic object, it cannot be said to be FN or TP. Thus, in the results, they are assumed to be False Classification (FC).

Object Detection Ratio (ODR) is the ratio of objects detected as in the dataset (TP+TN) to the total number of objects

$$ODR = \frac{TP + TN}{All\ \text{Objects}} = \frac{7910}{13900} = 56.9\% \quad (3)$$

Positive Object Discrimination (POD) is the ratio of TPs to the number of all positive objects. $(1156 + 85) = 1241$ of the positive images have been classified correctly. And, there are totally $(10 \times 310) = 3100$ positive objects used in 10 runs. This gives 40% Positive Object Discrimination accuracy.

$$POD = \frac{TP}{All\ Positives} = \frac{1156 + 85}{3100} = 40\% \quad (4)$$

False Alarm Rate (FAR) is the ratio of negative objects identified as positive (FP) to the total number of negatives.

$$FAR = \frac{FP}{All\ negatives} = \frac{1850 + 2281}{10800} = 38.3\% \quad (5)$$

Then, the Overall Performance can be defined as follows:

$$OP = \frac{(POD + ODR - FAR)}{2} \quad (6)$$

3.2 Implementation using KMeans

The implementation details described above have been used for three different image scales. Table 3 shows the results for KMeans for the test settings given. It can be seen from the table that there is high FAR ratio, except NRAS test settings. Secondly, usage of MM improves POD result. However, it also increases FAR and thus decreases ODR.

5-row average subtraction (5R) has provided the best Overall Performance (OP) with 55.2%. Because the POD results for NRAS are very low, 3RM can also be noted for its good result. At this test setting, POD increases from 25.2% to 63.2% and a relative increase in ODR is provided.

Table 3: The results for KMeans.

	POD	ODR	FAR	OP
NN	25.2%	66.5%	21.7%	35.0%
MM	35.5%	59.3%	33.9%	30.5%
1R	25.9%	83.5%	0.0%	54.7%
3R	25.9%	83.5%	0.0%	54.7%
5R	26.7%	83.7%	0.0%	55.2%
7R	25.9%	83.5%	0.0%	54.7%
3RM	63.2%	68.6%	29.9%	51.0%

The results for 1R, 3R and 7R are the same. But, 5-row average subtraction (5R) gives relatively better result than the others. Despite the results are low, application of NRAS and 3RM increases the OP notably. The low results are mostly because KMeans is an unsupervised clustering algorithm.

3.3 Using Support Vector Machines (SVM)

SVM is one of the most studied and well-known algorithms in Machine learning[23]. It provides linear and non-linear classification algorithms for both binary and multi-class representations. Original algorithm was proposed in 90s by Vapnik and Chervonenkis[24]. SVM creates a hyper-plane between the classes. When a new testing item is projected, the class is defined according to the position on the hyper-plane.

The method has been tested in using Rapidminer[25] toolbox, using 4 test settings with the following conditions. In the tests

- there are 310 positive and 1080 negative image crops,
- 60×90 image crops have been resized to 20%, 25% and 33%,
- 5-Fold cross validation has been used,
- libSVM from Rapidminer with the following parameters has been used:
  - SVM type: C-SVC,
  - Kernel type: linear,
  - C = 0,
  - Epsilon = 2,

where C is the cost and Epsilon is the tolerance of the termination criteria.

Table 4: The results for SVM.

	POD	ODR	FAR	OP
NN	37.85%	85.92%	0.28%	61.7%
MM	54.73%	89.78%	0.15%	72.2%
1R	74.09%	94.15%	0.09%	84.1%
3R	70.11%	93.21%	0.15%	81.6%
5R	69.25%	93.05%	0.12%	81.1%
7R	68.71%	92.95%	0.09%	80.8%
3RM	80.22%	95.42%	0.22%	87.7%

Table 4 shows the average results from 3 scales. Firstly, the results are better than the results using KMeans. The decrease in FAR is notable. Furthermore, the increase in POD and ODR did not increase FAR. And, FAR has decreased to 0.22%.

Similar to KMeans, usage of MM has provided some improvement on the results. And, application of NRAS has provided better results than MM. However, the best results have been achieved using 3RM. While the OP for NN is 61.7%, it increases to 81.6% with the application of 3R. 1R has produced better results than 3R and 5R. However, the best OP is provided by 3RM which reaches to 87.7%.

3.4 Using Artificial Neural Networks (ANN)

Artificial Neural networks (ANN)[26] is another very common Machine Learning algorithm. ANN aims to imitate brain neurons to reach the same brain power.

Four settings described in Section 3 have been used for Neural network tool from Rapidminer. The tool uses Sigmoid activation function by default. Then, the following properties have been selected for the tests:

- number of training cycles: 5,
- learning rate: 0.7,
- momentum: 0.7,
- error epsilon: 0.02,
- 2 hidden layers with 20 Nodes.

The results, presented in Table 5, are better than the results for SVM. Similar to KMeans 5R produce better results than other NRAS settings. Application of 5R has provided slightly better POD and ODR accuracies than NN. The application of 3RM has increased both POD and ODR results while providing a slender increase in FAR.

Table 5: ANN results

	POD	ODR	FAR	OP
NN	77.42%	94.82%	0.19%	86.0%
MM	78.17%	94.94%	0.25%	86.4%
1R	76.99%	94.82%	0.06%	85.9%
3R	78.82%	93.24%	2.62%	84.7%
5R	79.25%	95.37%	0.00%	87.3%
7R	78.06%	95.11%	0.00%	86.6%
3RM	87.74%	97.00%	0.34%	92.2%

ANN has provided better OP than the other two algorithms. Even though, the OP for NN is high, 86.0%, it reaches to 92.2% by the application of 3RM. And, this is the best overall performance among all three algorithms.

4. CONCLUSIONS

Landmine detection is still very important for many countries in the world. It requires fast and accurate detection performance. This paper proposes a method which provides fast processing while increasing the accuracy. The algorithm consists of three steps: NRAS, 2) Min-max normalization, 3) Image scaling. Application of the proposed method not only increases ODR and POD results in the tests but also provides better runtime performance.

The positive effect of NRAS is seen on all testing algorithms. For KMeans algorithm, although, Min-max normalization increases POD, but due to high FAR result, the ODR decreases to 59.3%. However, when 3RM is used, both ODR and POD results increase comparably. The high FAR rate for KMeans is due to the nature of the algorithm.

SVM increases POD from 37.85% to 80.22%. Moreover, it provides notably low FAR results compared to the other algorithms. Although, ANN has a bit higher FAR than SVM, it provides higher results than the other two testing algorithms.

According to our observation, the low results can be due to small data set used. Future studies will focus 3D datasets with more clutter and large number of TP objects. The experiment can give better opinion using 3D data.

REFERENCES

[1] R. Siegel, "Land Mine Detection," *IEEE Instrumentation & Measurement Magazine,* pp. 22-28, December 2002.

[2] U. Nations, "Landmines, mine action news from the united nations," United Nations, New York, 1998.

[3] H. Frigui and P. Gader, "Detection and discrimination of land mines in ground-penetrating radar based on edge histogram descriptors and a possibilistic k-nearest neighbor classifier," *IEEE Transactions on Fuzzy Systems,* vol. 17, no. 1, pp. 185-199, 2009.

[4] H. Frigui, P. Gader and K. Satyanarayana, "Landmine Detection with Ground Penetrating Radar using Fuzzy K-Nearest Neighbors," in *IEEE International Conference on Fuzzy Systems,* Budapest, 2004.

[5] K. C. Ho, P. D. Gader and J. N. Wilson, "Improving landmine detection using frequency domain features from ground penetrating radar," in *Geoscience and Remote Sensing Symposium, IEEE International,* Anchorage, AK, 2004.

[6] P. A. Torrione, C. S. Throckmorton and L. M. Collins, "Performance of an Adaptive Feature-Based Processor for a Wideband Ground Penetrating Radar System," *IEEE Transactions on Aerospace and Electronic Systems,* vol. 42, no. 2, pp. 644-658, 2006.

[7] H. Frigui, L. Zhang, P. Gader and D. Ho, "Context-dependent fusion for landmine detection with ground-penetrating radar," in *Defense and Security Symposium,* Orlando, FL, 2007.

[8] P. Gader, W. H. Lee and J. N. Wilson, "Detecting Landmines With Ground-Penetrating Radar Using Feature-Based Rules, Order Statistics, and Adaptive Whitening," *IEEE Transactions on Geoscience and Remote Sensing,* vol. 42, no. 11, pp. 2522-2534, 2004.

[9] A. K. Sinha and S. D. Mehta, "Detection of landmines," *Defence Science Journal,* vol. 51, no. 2, p. 115, 2001.

[10] D. J. Daniels, "Surface-penetrating radar," *Electronics & Communication Engineering Journal,* vol. 8, no. 4, pp. 165-182, 1996.

[11] M. Sezgin, F. Kurugollu, I. Tasdelen and S. Ozturk, "Real-time detection of buried objects by using GPR," in *Detection and Remediation Technologies for Mines and Minelike Targets IX*, Orlando FL, 2004.

[12] J. N. Wilson, P. Gader, W. H. Lee, H. Frigui and K. C. Ho, "A large-scale systematic evaluation of algorithms using ground-penetrating radar for landmine detection and discrimination," *IEEE Transactions on Geoscience and Remote Sensing,* vol. 45, no. 8, pp. 2560-2572, 2007.

[13] P. D. Gader, M. Mystkowski and Y. Zhao, "Landmine detection with ground penetrating radar using hidden Markov models," *IEEE Transactions on Geoscience and Remote Sensing,* vol. 39, no. 6, p. 1231—1244, 2001.

[14] H. Frigui and P. Gader, "Detection and discrimination of land mines based on edge histogram descriptors and fuzzy k-nearest neighbors," in *IEEE International Conference in Fuzzy Systems,* Vancouver, BC, 2006.

[15] P. A. Torrione, L. M. Collins, F. Clodfelter, F. Frasier and I. Starnes, "Application of the LMC algorithm to anomaly detection using the Wichmann/NIITEK ground-penetrating radar," in *AeroSense*, Orlando, FL, 2003.

[16] M. Sezgin, Y. Bahadirlar and I. Tasdelen, "Signal processing techniques to improve GPR detection performance," in *Detection and Remediation Technologies for Mines and Minelike Targets X*, Orlando, Florida, 2005.

[17] V. Munshi and L. M. Collins, "Physics model-based signal processing of gpr for subsurface object detection and discrimination," Department of electrical and computer engineering, Duke University, Durham, NC, 2003.

[18] A. S. Turk, "Ultra-wideband Vivaldi antenna design for multisensor adaptive ground-penetrating impulse radar," *Microwave and optical technology letters*, vol. 48, no. 5, pp. 834-839, 2006.

[19] C. R. Ratto, K. D. Morton, I. T. McMichael, B. P. Burns, W. W. Clark, L. M. Collins and P. A. Torrione, "Integration of lidar with the NIITEK GPR for improved performance on rough terrain," *SPIE Defense, Security, and Sensing*, vol. 5089, pp. 1375-1382, 2012.

[20] M. Iurlaro, G. Ficz, D. Oxley, E.-A. Raiber, M. Bachman, M. J. Booth, S. Andrews, S. Balasubramanian and W. Reik, "A screen for hydroxymethylcytosine and formylcytosine binding proteins suggests functions in transcription and chromatin regulation," *Genome Biology*, vol. 14, no. 10, p. R119, 2013.

[21] Z. Liu, F. Zhou, X. Chen, X. Bai and C. Sun, "Iterative infrared ship target segmentation based on multiple features," *Pattern Recognition*, vol. 47, no. 9, pp. 2839--2852, 2014.

[22] I. Mesecan and I. O. Bucak, "Searching The Effects of Image Scaling For Underground Object Detection Using KMeans And KNN," in *UKSim-AMSS 8th European Modelling Symposium*, Pisa, 2014.

[23] X. Wu and V. Kumar, The top ten algorithms in Data Mining, Boca Raton, London, New York: Chapman & Hall/CRC Taylor & Francis Group, 2009.

[24] V. N. Vladimir, Estimation of dependences based on empirical data, New York: Springer, 2006.

[25] M. Hofmann and R. Klinkenberg, RapidMiner: Data mining use cases and business analytics applications, CRC Press, 2013.

[26] G. Zakar, Artificial Neural Networks, CreateSpace Independent Publishing Platform, 2016.

Contributors

Assoc. Prof. Dr. İhsan Ömür Bucak obtained his BS and MS, Istanbul Technical University, PhD, Oakland University, Rochester, Michigan, 2000. Research strength mainly lies on Control Systems, Signal Processing, Artificial Intelligence, and Bioinformatics. His special interests are Hybrid Electric Vehicles and Powertrain Controls. He has 7 years of industrial experience in this area all in the U.S. He is currently working in Academia and a full-time Associate Professor at Meliksah University, Kayseri-Turkey since the year of 2013. He is teaching undergraduate courses such as Signals and Systems, Communication Systems and Control Systems at Electrical and Electronics Engineering Department.

MSc. İbrahim Meşecan obtained his MSc. in Software engineering in 1999. He works as a lecturer at Epoka University, Tirana, Albania since 2011. And, he is a PhD. student at Mevlana university Konya, Turkey since 2012. He has published three research articles and three books. His main interests are Computer Vision and Pattern Recognition.